Diurnal Cycle of Convection during the 2004 North American Monsoon Experiment

RICHARD H. JOHNSON, PAUL E. CIESIELSKI, TRISTAN S. L'ECUYER, AND ANDREW J. NEWMAN

Department of Atmospheric Science, Colorado State University, Fort Collins, Colorado

(Manuscript received 2 June 2009, in final form 16 September 2009)

ABSTRACT

The diurnal cycle of summer monsoon convection in the coastal, mountainous region of northwestern Mexico is investigated using data from the 2004 North American Monsoon Experiment (NAME). Data from a special sounding network consisting of research and operational sites have been quality controlled and combined with surface, wind profiler, and pibal observations to create a gridded dataset over the NAME domain. This study concentrates on results from the interior portion of the NAME sounding network, where gridded analysis fields are independent of model data. Special attention is given to surface and pibal observations along the western slope of the Sierra Madre Occidental (SMO) in order to obtain an optimal analysis of the diurnally varying slope flows.

Results show a prominent sea-breeze–land-breeze cycle along the western slopes of the SMO. There is a deep return flow above the afternoon sea breeze as a consequence of the elevated SMO immediately to the east. The upslope flow along the western slope of the SMO is delayed until late morning, likely in response to early morning low clouds over the SMO crest and reduced morning insolation over the west-facing slopes. The diurnal cycle of the net radiative heating rate is characterized by a net cooling during most of the daytime except for net heating in the lower and upper troposphere at midday. The diurnal cycle of the apparent heat source Q_1 minus the radiative heating rate Q_R (providing a measure of net condensational heating) and the apparent moisture sink Q_2 over the SMO is indicative of shallow convection around noon, deep convection at 1800 LT, evolving to stratiform precipitation by midnight, consistent with the radar-observed diurnal evolution of precipitation over this coastal mountainous region as well as the typical evolution of tropical convective systems across a wide range of spatial and temporal scales. Convection over the Gulf of California is strikingly different from that over land, namely, heating and moistening are confined principally to the lower troposphere below 700 hPa, peaking during the nighttime hours.

1. Introduction

The diurnal cycle is a dominant feature of monsoon regions of the world. Within the largest monsoon system—the Asian monsoon—the Tibetan Plateau generates significant, large-scale, diurnally varying circulations, vertical motion, and diabatic heating (Luo and Yanai 1984; Nitta 1983; Krishnamurti and Kishtawal 2000). The North American summer monsoon system, which develops in response to heating over the elevated terrain of Mexico and the western United States (Krishnamurti 1971), also exhibits diurnally driven large-scale circulations similar to those over Asia (Tang and Reiter 1984; Tucker 1999). Embedded within these larger-scale circulation features are diurnally forced mesoscale flows, such as land–sea and mountain–valley winds, which control the location and timing of convective precipitation in the monsoons of Asia (Johnson 2006) and North America (Douglas et al. 1993; Dai et al. 1999). The 2004 North American Monsoon Experiment (NAME) was designed, in part, to investigate the diurnal cycle of precipitation during the summer monsoon in the coastal, mountainous region of northwestern Mexico (Higgins et al. 2006).

Understanding the diurnal cycle of precipitation in monsoon regions is important because much of the world's precipitation occurs there and global models do not properly represent its diurnal phase and amplitude (Yang and Slingo 2001; Slingo et al. 2003; Neale and Slingo 2003; Gutzler et al. 2005). As noted by Sperber and Yasunari (2006), the diurnal cycle impacts processes on the intraseasonal time scale, thereby complicating the treatment of the Madden–Julian oscillation (MJO; Madden and Julian 1971). The diurnal cycle of rainfall is

Corresponding author address: Richard H. Johnson, Department of Atmospheric Science, Colorado State University, Fort Collins, CO 80523.
E-mail: johnson@atmos.colostate.edu

DOI: 10.1175/2009JCLI3275.1

particularly prominent in coastal and mountainous areas of the monsoon regions and Indonesian Maritime Continent (Janowiak et al. 2005). While observations of the diurnal cycle of convection have increased dramatically during the past decade, clarification of the mechanisms has remained elusive. Over the open ocean, an early-morning maximum of precipitation has generally been observed. This behavior has been attributed to a variety of processes acting singly or in combination: horizontal gradients in radiative cooling between cloud systems and their environment (Gray and Jacobson 1977), daytime stabilization of the upper troposphere by shortwave heating and destabilization at night by longwave cooling (Kraus 1963; Randall et al. 1991), and the life cycle effects of mesoscale convective systems (Chen and Houze 1997). Over land, daytime heating exerts the primary control on the diurnal cycle of precipitation; however, factors influencing the development and organization of convection—surface fluxes, surface heterogeneity, low-level jets, orography, convective downdrafts, etc.—are varied and complex, complicating its treatment in models (Betts and Jakob 2002; Bechtold et al. 2004: Khairoutdinov and Randall 2006).

Observations prior to NAME have revealed prominent summertime land–sea and mountain–valley breeze circulations and precipitation patterns over northwestern Mexico characterized by a vigorous diurnal cycle along and to the west of the Sierra Madre Occidental (SMO). Many details of the surface circulation and its diurnal cycle are poorly represented in a version of the North American Regional Reanalysis (NARR) especially prepared for NAME (Mo et al. 2007; Ciesielski and Johnson 2008). In response to insolation and local thermally forced circulations, convection typically initiates over the higher terrain of the SMO during the afternoon and intensifies and moves westward during the evening toward the coastline of the Gulf of California (GoC), eventually dissipating during the early morning (Stensrud et al. 1995; Gochis et al. 2003; Janowiak et al. 2005). Such behavior was also found during NAME by Lang et al. (2007) using data from a multiradar network along the west coast of Mexico, who also noted that convection frequently organized into mesoscale convective systems (MCSs) on its trek toward the coastal plain. However, on some occasions, westward motion was restricted and convection moved from south to north along the SMO. In addition, there were times when enhanced convection occurred along the coast and over the GoC, especially overnight and in the early morning. The diurnal evolution of convection over the SMO has been analyzed in detail by Nesbitt et al. (2008) using rain gauge, radar, and satellite data. They find shallow, nonprecipitating stratus clouds to exist over the high terrain of the SMO at night, which evolve into shallow convection just after local noon. Thereafter, convection deepens and organizes into MCSs as it propagates onto the coastal plain where it dissipates rapidly. The diurnal cycle of convection has also been analyzed by Negri et al. (1993) and Rowe et al. (2008), who found important differences in the diurnal frequency and intensity of precipitation in different elevation zones along the SMO.

The NAME sounding network represents the first intensive sounding array that has been established in a coastal, mountainous region to study monsoon convection. It has sufficient temporal and spatial resolution during intensive observing periods to investigate the diurnal evolution of the flow and the vertical distribution of heat sources and moisture sinks over both land and ocean, which are the objectives of this study. Determination of the vertical profile of heating in the NAME monsoon region is important since there is considerable uncertainty in this profile based on models and large-scale circulation is sensitive to the vertical heating distribution (Barlow et al. 1998). Isolation of the latent heating contribution to the total diabatic heating is aided in this study by employing independent estimates of the net radiative heating profiles using the methodology introduced by L'Ecuyer and Stephens (2003, 2007). To summarize the methodology of this paper, we use gridded analysis fields produced primarily from the sounding data and estimates of radiative heating rates to document the diurnal cycle of the kinematic and thermodynamic features of the flow and the latent heating and moistening distributions over the NAME domain.

2. Data and analysis procedures

a. Sounding data

The NAME sounding network utilized in this study (Fig. 1) features two nested domains: the Tier I Array (T1A), covering the core NAME region where precipitation is modulated by the North American monsoon; and the Enhanced Budget Array (EBA), where a denser network of soundings was established to capture heat and moisture budgets in proximity to the rain gauge and radar networks. T1A consists of operational sounding sites of the U.S. Weather Service and the Mexico Weather Service [Servicio Meteorológico Nacional (SMN)], some of which increased their launch frequency during the intensive observing periods (IOPs) of NAME, and five additional sounding sites established along the GoC (Puerto Peñasco, Bahia Kino, Los Mochis, Loreto, and the R/V *Altair*). In the EBA, up to six

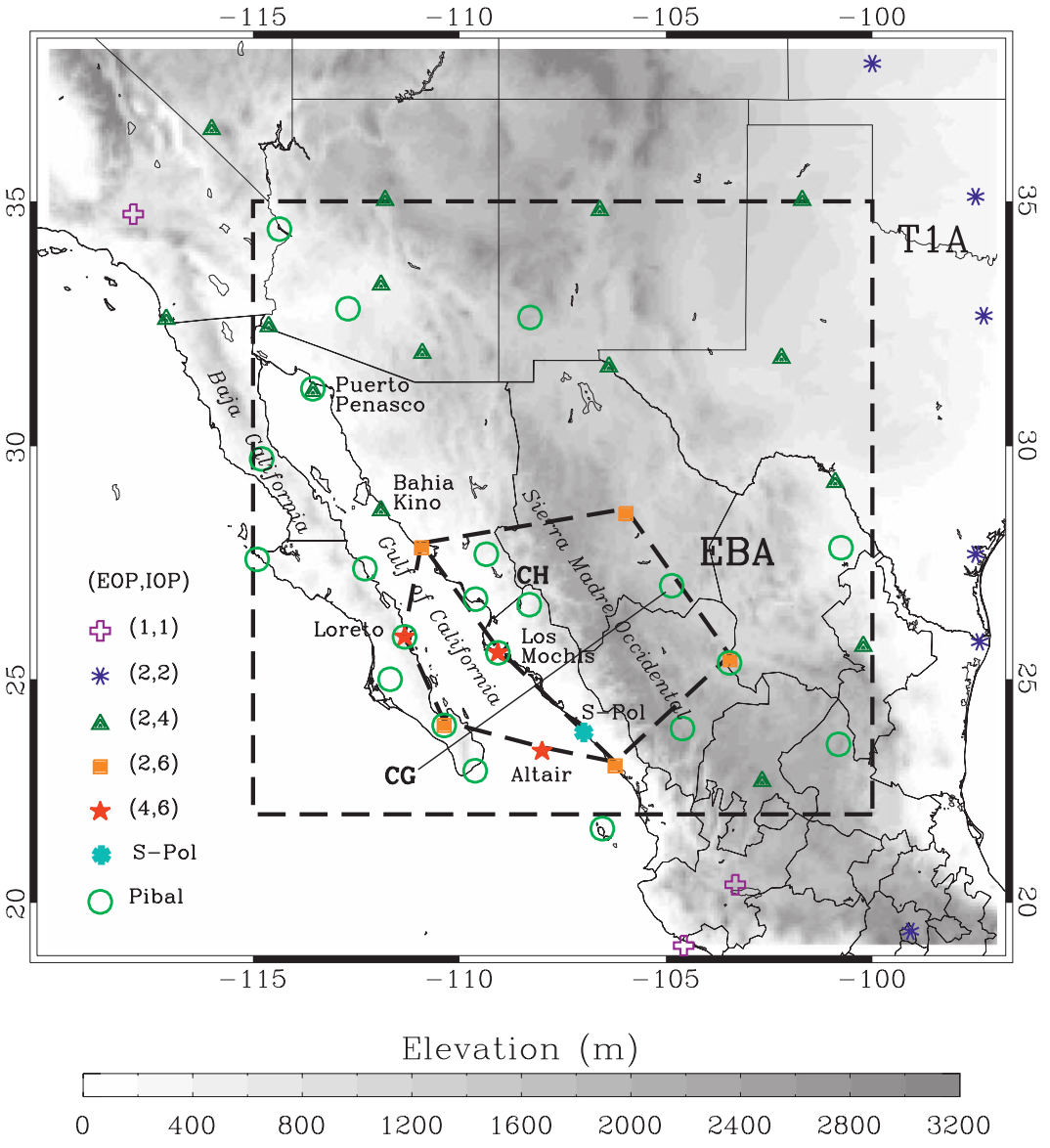

FIG. 1. NAME sounding network and two grids used for sounding analysis: Tier I Array (T1A) and EBA. Symbols indicate frequency of routine sounding launches (left number) and frequency of increased sounding launches (right number) during IOPs, as well as S-Pol radar site. Budgets are computed separately for the overwater and overland portions of the EBA. Line segment CG refers to axis of cross-gulf vertical cross sections used in subsequent figures.

soundings per day were obtained during IOPs in order to study the diurnal cycle of the flow and convection in the vicinity of the SMO both when significant weather events were occurring and during undisturbed conditions. The launch frequencies for these sites during the interval encompassing the IOPs, 7 July–15 August, are indicated in Fig. 1. Sounding quality control procedures are described in Johnson et al. (2007). In addition to those procedures, a statistical correction technique developed by Ciesielski et al. (2009) to remove dry biases associated with Vaisala RS80-H sondes has been applied to the humidity data taken during NAME.

The National Center for Atmospheric Research (NCAR) S-Band polarimetric (S-Pol) research radar operated within the budget polygon during the period of NAME IOPs. In addition, NCAR Integrated Sounding Systems (ISSs), consisting of Vaisala GPS sounding systems, 915-MHz wind profilers, radio acoustic sounding systems (RASSs), and surface meteorological stations, were operated at Puerto Peñasco, Bahia Kino, and

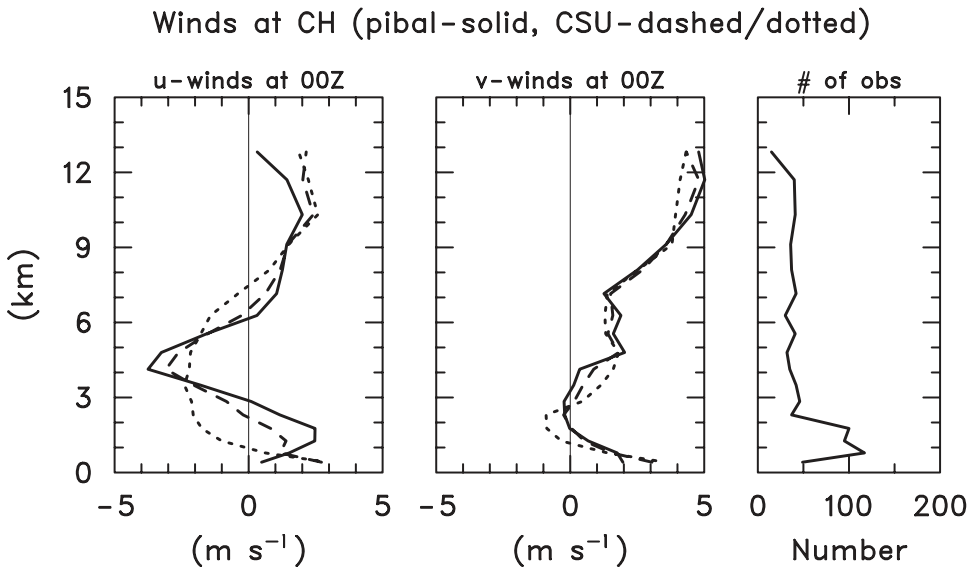

FIG. 2. Average zonal and meridional (u and v) wind profiles at pibal site at Choix (CH, see Fig. 1 for location) during 1 Jul–15 Aug 2004 NAME observing period (solid curves) and at grid point nearest Choix from gridded analysis of sounding data excluding pibals (dotted curves) and including pibals (dashed curves). (right) Number of pibal observations as a function of height.

Los Mochis. The ISSs provided high-time-resolution (30 min) wind profiles reliably in the lowest 2–3 km of the atmosphere. Finally, 21 pibal sounding sites were operated within the NAME region (Fig. 1), whose impacts on the analyses are discussed below.

b. Impact of pibal data regional analysis of diurnal cycle

The pibal data (winds as a function of height) collected during NAME were part of the Pan American Climate Studies Program-Sounding Network (PACS-SONET; Douglas and Murillo 2008). During NAME, nearly 1000 pibal soundings were taken within or in close proximity to the EBA (locations indicated in Fig. 1). All pibal soundings were taken during the daytime, with the majority (more than 90%) in 2-h periods centered around 0800 and 1800 LT. To illustrate the impact of the pibal data on analysis of the diurnal cycle, a comparison of the average u and v components of the flow at 0000 UTC (1800 LT) at the pibal site CH on the coastal plain just northeast of Los Mochis (Fig. 1) with those obtained from the gridded analysis (with and without pibal data) described in section 2e is presented in Fig. 2. The gridded analysis *without* pibal data is not able to properly capture the low-level jet between 1 and 2 km associated with the afternoon sea breeze and also does not properly depict the easterly jet between 4 and 5 km. However, the gridded analysis *with* pibal data better represents the pibal wind profiles.

c. Computation of heat and moisture budgets and radiative heating rates

The apparent heat source and moisture sink (Yanai et al. 1973) are defined by

$$Q_1 \equiv \frac{\partial \overline{s}}{\partial t} + \overline{\mathbf{v}} \cdot \nabla \overline{s} + \bar{\omega} \frac{\partial \overline{s}}{\partial p} = Q_R + L(\overline{c} - \overline{e}) - \frac{\partial \overline{\omega' s'}}{\partial p}, \quad (1)$$

$$Q_2 \equiv -L\left(\frac{\partial \overline{q}}{\partial t} + \overline{\mathbf{v}} \cdot \nabla \overline{q} + \bar{\omega} \frac{\partial \overline{q}}{\partial p}\right) = L(\overline{c} - \overline{e}) + L \frac{\partial \overline{\omega' q'}}{\partial p}, \quad (2)$$

where $s = c_p T + gz$ is the dry static energy, q is the water vapor mixing ratio, c is the condensation rate, e is the evaporation rate, L is the latent heat of vaporization, c_p is the specific heat of dry air, Q_R is the radiative heating rate, the overbar denotes an area average, and the prime represents a departure from that average. Both Q_1 and Q_2 are computed using gridded sounding data. Ciesielski et al. (2009) showed that while corrections to the Vaisala RS80-H dry biases during NAME had little effect on the time-mean Q_2, they had an important impact on its diurnal cycle. Those corrections are used in this paper.

In this study Q_R estimates are derived from an approach known as the Hydrologic cycle and Earth's Radiation Budget (HERB) algorithm (L'Ecuyer and Stephens 2003, 2007). HERB synthesizes ice cloud microphysical property information from the Visible and Infrared Scanner (VIRS); liquid cloud properties, precipitation

profiles, SST, and water vapor retrievals from the Tropical Rainfall Measuring Mission (TRMM) Microwave Imager (TMI); and vertical profiles of temperature and humidity from the National Centers for Environmental Prediction (NCEP) reanalyses, to characterize the three-dimensional structure of clouds and precipitation in the atmosphere. Aerosols are prescribed using a static climatology of monthly distributions from the Global Aerosol Climatology Project (GACP). These fields provide input to a broadband radiative transfer model that simulates vertical profiles of upwelling and downwelling longwave and shortwave radiative fluxes and their convergence defines the vertical profile of atmospheric radiative heating Q_R. A comprehensive description of the uncertainty characteristics of the HERB products has been prepared by L'Ecuyer and McGarragh (2010). Uncertainties tend to be a strong function of time and space scale but, for reference, monthly, 5° top-of-the-atmosphere outgoing longwave and shortwave flux estimates agree with corresponding observations from the Clouds and the Earth's Radiant Energy System (CERES) to within 7 W m^{-2} and 3%, respectively.

Considering the short 40-day time period of the NAME observations, Q_R has been also computed for the NAME domain using data for the 10-yr 1998–2007 period of TRMM. The results are similar for both periods, but since there is more confidence in the 10-yr averages, we use the longer time period in the subsequent analyses.[1] The Q_R from the HERB algorithm is provided at 0.5° horizontal, 1-km vertical resolution from 0.5 to 17.5 km above the ground. These data, for the period 7 July–15 August 1998–2007, were extracted over the NAME T1A domain (Fig. 1). They were then binned by time of day, adjusted to be a function of height above sea level using a 0.5° resolution topographic dataset, and then averaged over the land and gulf portions of the EBA.

d. Other data sources

Surface winds over the GoC and the eastern Pacific are obtained from National Aeronautics and Space Administration (NASA) Quick Scatterometer (QuikSCAT), which provides wind estimates nominally twice per day at 25-km horizontal resolution (Liu 2002). Precipitation estimates at 3-h intervals, 0.25° resolution are based on the TRMM 3B42v6 algorithm (Huffman et al. 2007). For the exterior portions of the analysis domain, model data from a special version of the NARR prepared for NAME (Mo et al. 2007) are used. The resolution of the NARR product is 32 km, 45 vertical levels, and 3 h.

e. Objective analysis

In this study gridded fields of horizontal wind components u and v, temperature T, water vapor mixing ratio q, and geopotential height z at 1° horizontal and 25-hPa vertical resolution have been computed from the quality-controlled sounding and pibal data using the multiquadric interpolation scheme of Nuss and Titley (1994). Additional details of the procedure can be found in Ciesielski et al. (2003). For the 40-day period with intensive observations from 7 July to 15 August, gridded analyses were computed at 0000, 0600, 1200, and 1800 UTC over the T1A domain shown in Fig. 1. To aid the T1A analysis at 0600 and 1800 UTC on non-IOP days, time-interpolated sondes and profiler data from the ISS sites were used. On IOP days (12–15, 20–23, and 28–30 July; 1–8 and 10–14 August), gridded analyses were produced at 0000, 0400, 0800, 1200, 1600, and 2000 UTC over a domain slightly larger than the EBA from 23°–29°N to 103°–112°W. Owing to the oceanic data-void regions outside T1A, grid points over the eastern Pacific and Gulf of Mexico were assigned values given by the NARR. *However, we emphasize that this procedure to enhance the data field was only applied to large-scale analyses outside the main area of focus, the EBA, so the results in this interior domain are virtually independent of model data.* In addition, analysis at the surface included observations from METAR stations and QuikSCAT winds over the oceans when available.

The vertical p-velocity ω used in computing the atmospheric budgets was obtained through the kinematic method where horizontal divergence is integrated upward starting at the surface. The vertical motion at the surface was computed using the objectively analyzed surface winds and the terrain slope following the procedure of Ciesielski and Johnson (2008). The divergence field is mass balanced in the vertical by assuming adiabatic flow at the tropopause and using a constant divergence correction as suggested by O'Brien (1970). Details on the computation of the apparent heat source Q_1 and apparent moisture sink Q_2 can be found in Johnson and Ciesielski (2000).

3. Temporal variability of vertical motion over the 40-day period of NAME

Time series of daily-averaged vertical motion for the period 7 July–15 August are shown in Fig. 3 for both the land and ocean portions of the EBA. Also indicated in this figure are the nine IOPs that occurred during this

[1] Comparisons of q from the NCEP reanalyses and the gridded analyses show differences up to 10% on the time scales over which the Q_R data have been averaged. Based on sensitivity studies similar to those outlined in L'Ecuyer and Stephens (2003), these differences could introduce errors of up to 5% in the TRMM longwave and 2% in the shortwave heating rate estimates.

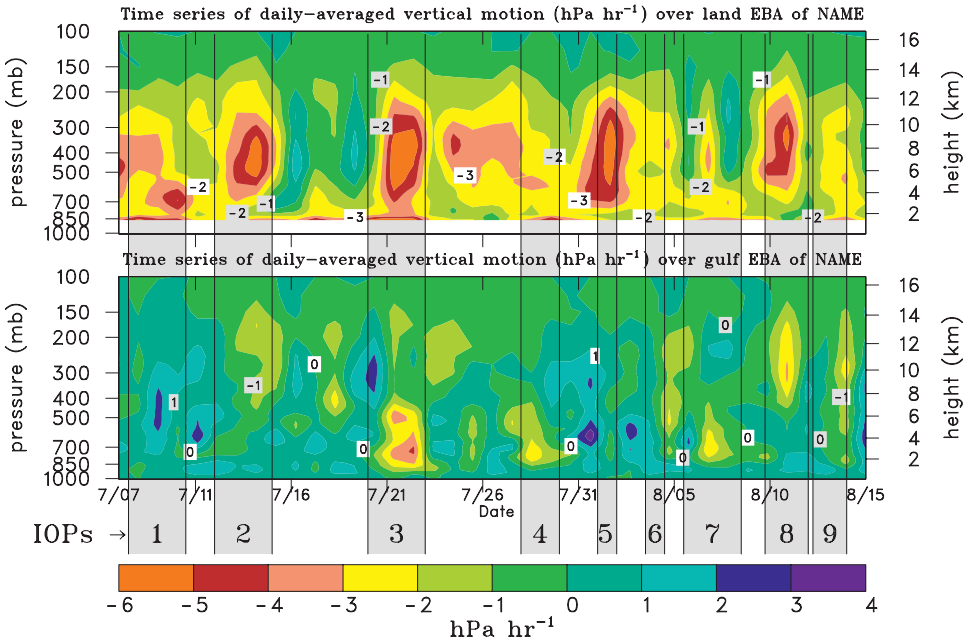

FIG. 3. Time series of vertical motion (hPa h^{-1}) from 7 Jul to 15 Aug 2004 over the (top) land and (bottom) ocean portions of the EBA. Vertical gray shadings mark IOPs.

period. The results over the land area (top panel) indicate that the IOPs did a fairly good job of capturing the majority of the episodes of upward vertical motion associated with deep convection, as discussed in Johnson et al. (2007). In IOPs 2, 3, 5, and 8, there is a slight indication that upward motion first peaked in the lower troposphere, followed by a peak in the mid- to upper troposphere at a later time. This evolution from shallow to deep convection during these 2–3-day convective episodes has been identified as a recurring feature of deep convective systems on multiple time and spatial scales, ranging from mesoscale convective systems to the Madden–Julian oscillation (see Kiladis et al. 2009 for a review).

Over the ocean portion of the EBA (bottom panel, Fig. 3), upward motion was far weaker and more erratic in terms of the height of the peak upward motion than over land, although there was still some correspondence between increased upward motion and IOPs. Consistent with the weaker vertical motion, the ocean area received far less precipitation than over land, as can be seen from Fig. 4 (discussed in section 4).

4. Diurnal cycle of the circulation and precipitation on the regional scale

Ciesielski and Johnson (2008) documented the diurnal variability of the surface flow over northwestern Mexico using surface station data over land and QuikSCAT data over the ocean.[2] The surface circulation is further analyzed in Fig. 4, a depiction of the 40-day mean (7 July–15 August) diurnal cycle of the surface flow and precipitation from the TRMM 3B42v6 product.

At 0600 LT (Fig. 4, top-left panel) the flow over most of the land area of northern Mexico is easterly and converges along the west coast with westerly flow crossing the GoC. The confluence axis (also a convergence axis, not shown) is consistent with coastal precipitation observed at this time. By noon, the coastal confluence line has moved to near the SMO crest, where precipitation is beginning to develop. Precipitation intensifies markedly by 1800 LT and moves toward the coastal plain, while the analyzed confluence line still remains over and to the east of the SMO crest. The analysis of the surface flow confluence line over north-central Mexico to the east of the SMO crest at this time is judged to be unreliable because of the sparsity of observations in this region (Ciesielski and Johnson 2008, their Fig. 1). By midnight, the precipitation weakens along the coastal plain, with a confluence axis generally aligned along the precipitation

[2] It was found that for a 10-day period in July prior to the monsoon-related vegetation green-up over land, there is a prominent afternoon sea breeze extending 300–400 km offshore along the coastal plain to the west of the SMO. The offshore extent of the sea breeze was found to be greater prior to green-up than afterward, suggesting that the growth of vegetation after monsoon onset reduced the land–sea temperature contrast.

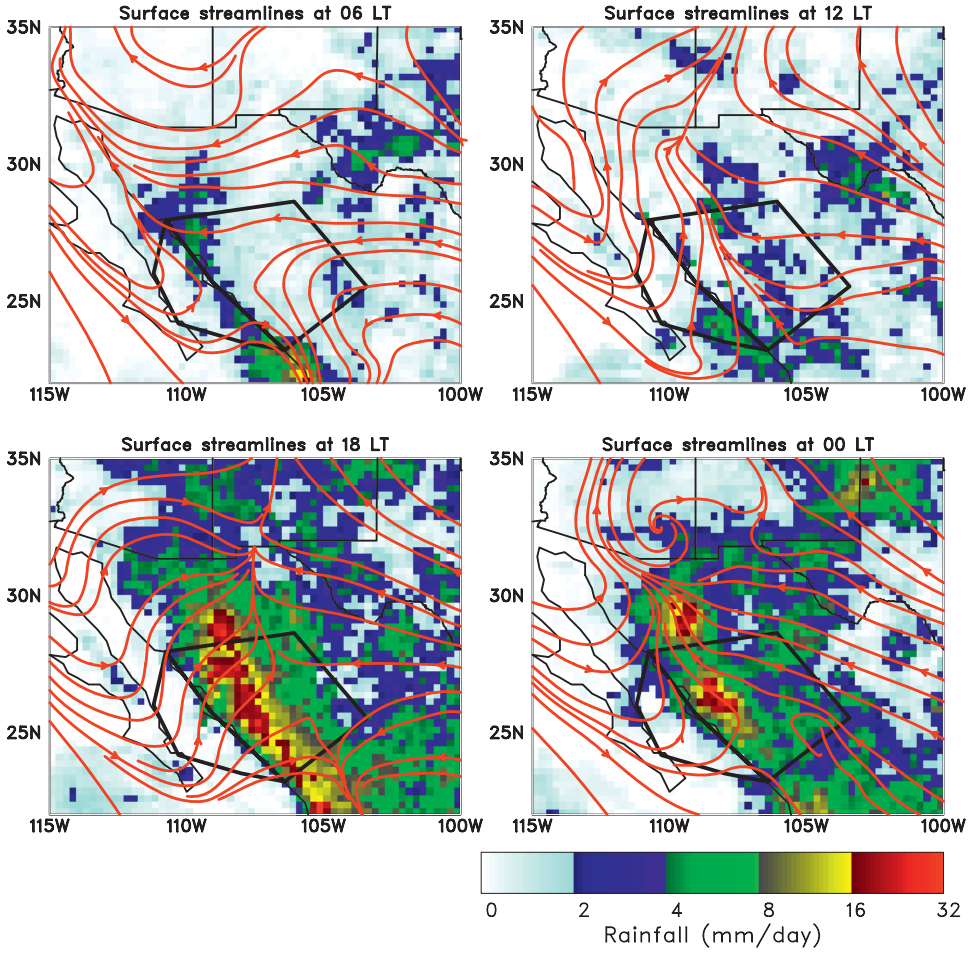

FIG. 4. The 40-day mean (7 Jul–15 Aug 2004) surface streamlines and rainfall rate from the TRMM 3B42v6 product at 0600, 1200, 1800, and 0000 LT. Black polygon denotes EBA.

maximum. At this time, there is a greater density of surface observations along the confluence axis. Overall, the analyzed pattern of the diurnal cycle of the surface winds is consistent with the diurnal cycle of precipitation.

In Fig. 5, the diurnal cycle of the 40-day mean vertical motion ω at 500 hPa is shown along with precipitation rate. Owing to the sparsity of soundings (Fig. 1), ω is least reliable on the western, eastern, and southern edges of the domain. In the early morning (0600 LT), the primary precipitation region along the coastline is accompanied by only spotty upward motion areas. By noon, the pattern of vertical motion is relatively weak, although some upward motion is diagnosed near the mouth of the GoC and inland from there where precipitation is occurring. By 1800 LT, strong upward motion is diagnosed coincident with the intense precipitation over the coastal plain. As this precipitation weakens by midnight, weaker upward motion is observed centered on the heaviest rainfall areas. A persistent area of upward motion in proximity to the northern GoC is considered unreliable because of the lack of soundings over northern Baja California (Fig. 1).

The diurnal cycle of precipitation during NAME is shown in a broader-scale context in Fig. 6, the 10-yr (1998–2007) July–August average time in the diurnal cycle of maximum precipitation based on the TRMM 3B42v6 product. Although the temporal resolution of this product is only 3-hourly, the results show rainfall along the axis of the SMO peaking around 1800 LT, with progressively later maxima (toward midnight) near the GoC coastline. Nocturnal maxima are observed at most locations all along the western Mexico coastline, with a clear signal of offshore motion south of the mouth of the GoC at an inferred speed of $\sim$15 m s^{-1}, similar to offshore-propagation speeds found over the Panama Bight by Mapes et al. (2003), over the Bay of Bengal by Yang and Slingo (2001) and Webster et al. (2002), and over the northern and southern South China Sea by

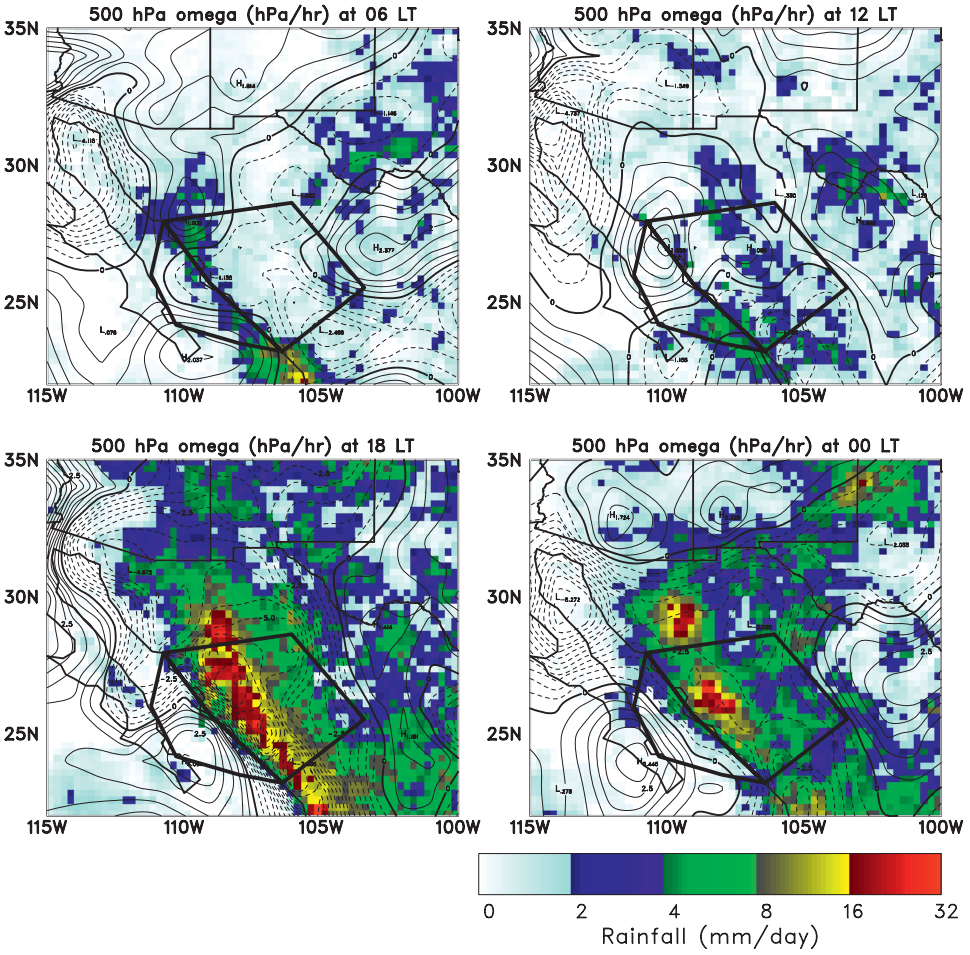

FIG. 5. The 40-day mean (7 Jul–15 Aug 2004) vertical p velocity (contour interval: 0.5 hPa h^{-1}) and rainfall rate from the TRMM 3B42v6 product at 0600, 1200, 1800, and 0000 LT. Dashed (solid) contours denote upward (sinking) motion. Black polygon denotes EBA.

Aves and Johnson (2008) and Ciesielski and Johnson (2006). Also evident in Fig. 6 is the strong signal of eastward propagation of convection from the Rocky Mountains over the central plains of the United States (Wallace 1975; Carbone et al. 2002).

5. Cross-gulf transects of the diurnal cycle of the flow on 18 IOP days

To examine the diurnal cycle of the flow along the SMO and coastal plain, vertical cross sections of winds, potential temperature, and relative humidity (corrected for dry biases as described by Ciesielski et al. 2009) have been constructed normal to the SMO across the center of the EBA (averages within 1° of line CG in Fig. 1) and extending across the Baja Peninsula. Owing to the lack of sounding data to the west of the Baja Peninsula (Fig. 1), the portion of the cross sections over Baja is influenced significantly by insertion of NARR data in the eastern Pacific, so analyses in these regions will not be discussed. Attention will be focused on the flow over the SMO and coastal plain, where analyses are not impacted by the use of NARR data over the eastern Pacific. When interpreting the results in this region, we caution that the confinement of sounding sites to coastal stations and stations east of the SMO limits the ability of analyses to accurately describe all details of the flow over the interior. However, the existence of surface stations over the interior (Ciesielski and Johnson 2008, their Fig. 1) as well as some pibal sites (Fig. 1), greatly assists analyses along the coastal plain and over the SMO.

The diurnal cycle of the flow on the 18 IOP days when there were six soundings per day is shown in Fig. 7. At 0200 LT, moist, easterly flow aloft can be seen over the SMO, the moist air being a result of the remnants of convection from the previous evening (Fig. 4). Downslope flow exists on the western slope of the SMO at 0200 and 0600 LT, and continues until 1000 LT, despite the fact

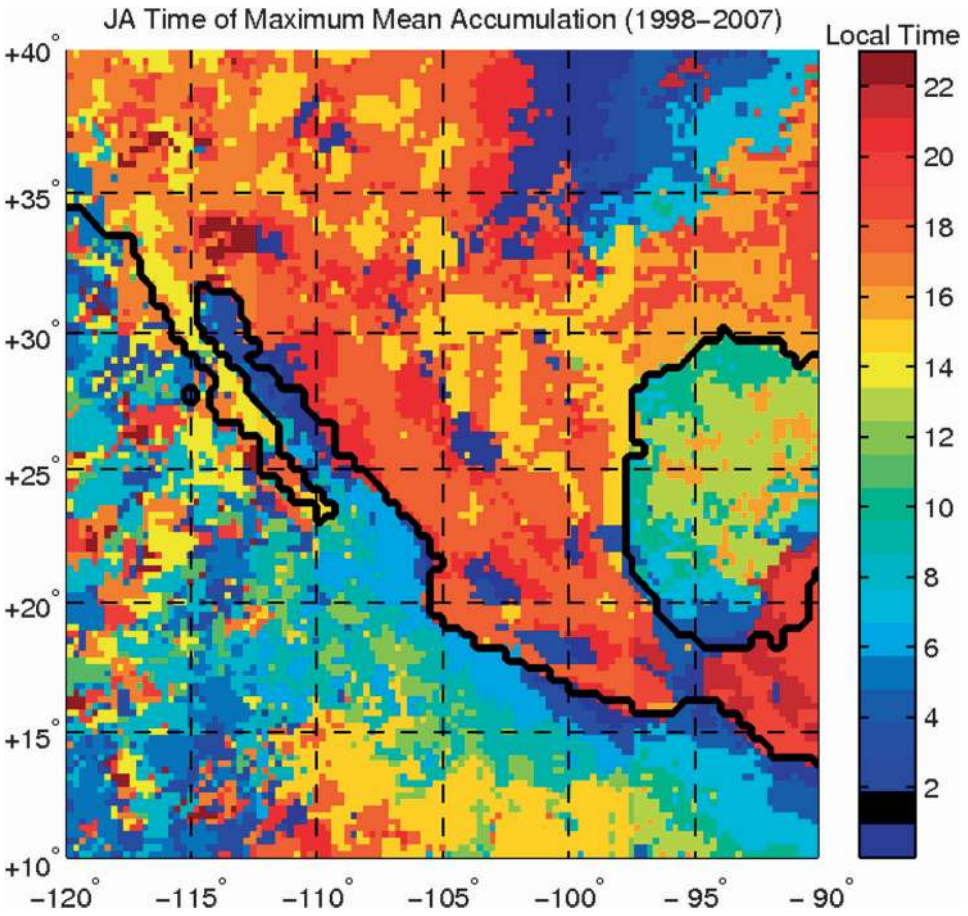

FIG. 6. The 10-yr average (1998–2007) time of maximum rainfall accumulation based on 3-hourly data from the TRMM 3B42v6 product.

that heating of the SMO crest is observed at 1000 LT as evidenced by the potential temperature field. Upslope flow has already begun on the eastern slope by this time.[3] This asymmetry in the development of the upslope flows may be related to insolation asymmetry for the north–south SMO barrier and also to the presence of low-level clouds in the morning along the high western slopes, which may retard surface heating at that time (Ciesielski and Johnson 2008; Nesbitt et al. 2008). However, by 1400 LT, upslope flow has developed on the western slope as heating over the crest intensifies. The flow at this time, characterized by a deep rotorlike circulation downstream of the SMO, closely resembles the mean circulation in this region obtained by Stensrud et al. (1995) in a 32-day summer monsoon simulation; however, they do not display results for the diurnal cycle. Also at 1400 LT, there is a switchover from downward to upward motion just downstream of the SMO, consistent with the development of convection over the barrier at this time. By 1800 LT, strong upward motion is seen over the western slope of the SMO, although an accompanying moist column is not evident at this time. This result is a clear deficiency in the analysis, reflecting the fact that at this time the sounding sites along the coast and east of the SMO cannot capture the moistening by deep convection over the SMO in the interior of the domain. At 2200 LT, upper-level moistening is finally observed and the low-level upslope flow in the afternoon/evening begins to revert to a downslope flow.

[3] There are limited surface observations east of the SMO crest (Ciesielski and Johnson 2008), so there is less confidence in the diurnal cycle of the surface flow depicted there in Fig. 7.

6. Diabatic heating profiles

a. Diurnal cycle of radiative heating rates

The diurnal cycle of the radiative heating rates based on 10 yr of TRMM data for the same 40-day period of NAME are shown in Fig. 8 for both the Gulf and land portions of the EBA. There is net column cooling throughout most of the day over both land and water,

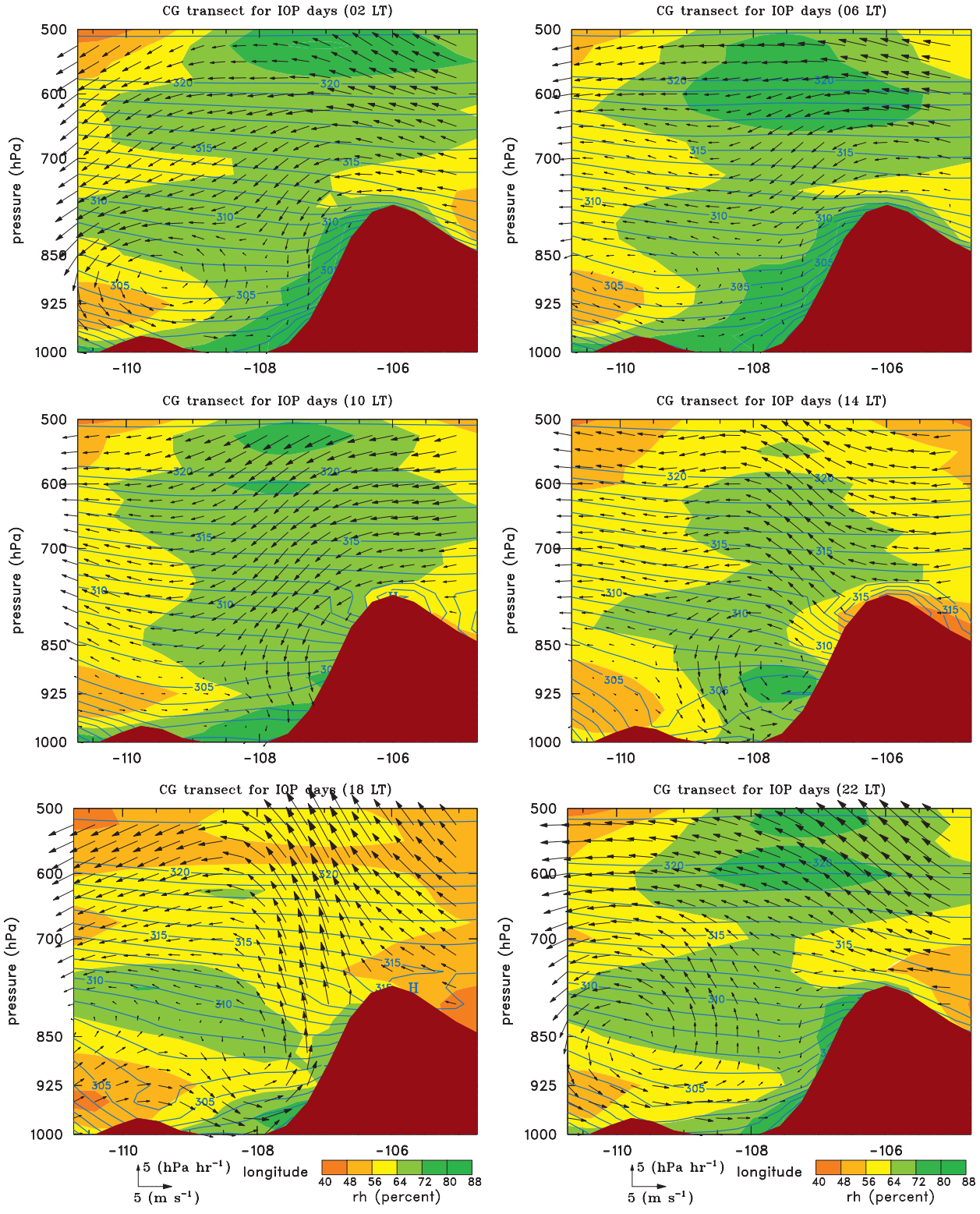

FIG. 7. Diurnal cycle of cross-gulf transect of relative humidity (shaded contours with scale at bottom) averaged over 18 IOP days during NAME. Blue lines are isentropes (1-K increment below 320 K and 5 K above) and arrows denote wind flow in the plane of transect (scale shown at bottom). Analysis uses NARR west of Baja.

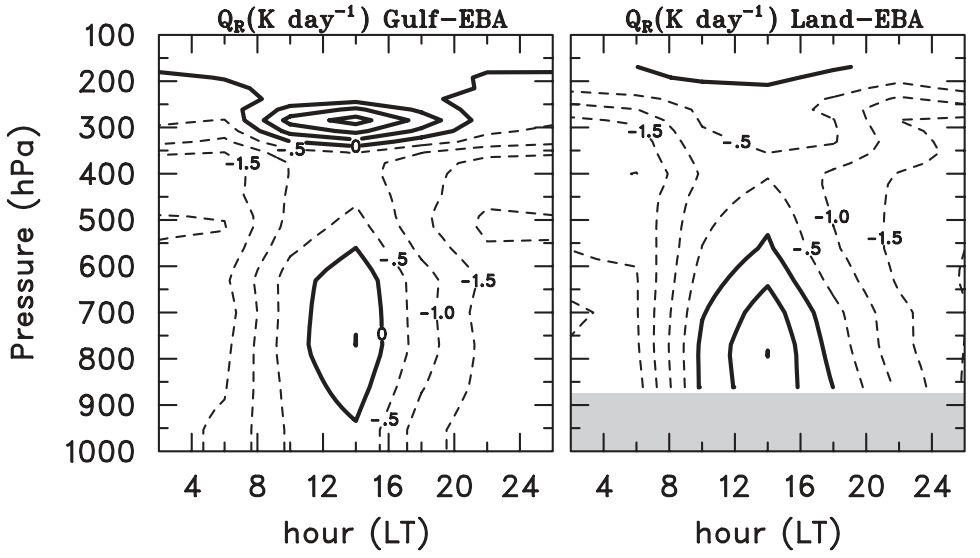

FIG. 8. Diurnal cycle of the net radiative heating rate over the Gulf and land portions of the EBA depicted in Fig. 1 based on the period 7 Jul–15 Aug 2004 and binned at 4-h intervals for the 1998–2007 years of TRMM. (right) Shaded area depicts average height of terrain.

except at midday in the upper and lower troposphere. The radiative heating in the lower troposphere during the daytime is principally a result of shortwave water vapor absorption with a minor contribution due to aerosols. Net heating in the upper troposphere is seen over both land and ocean, but is more intense and at a lower level over the water. This difference can be explained by the fact that there is longwave cooling atop deep convection offsetting shortwave absorption over land, whereas over the ocean there is only thin cirrus aloft advected westward from deep convection over the SMO, yielding a net heating (Webster and Stephens 1980; Ackerman et al. 1988).

Cross-gulf transects of the diurnal cycle of radiative heating rates based on the 10-yr period, along with relative humidity and potential temperature for the NAME 40-day period, are shown in Fig. 9. Near sunrise, at 0600 LT, there is net cooling at almost all levels. At noon, net heating develops in the lower troposphere, which is slightly stronger over the land areas. Net heating is also present in the upper troposphere centered between 200 and 250 hPa to the west of the SMO, presumably associated with thin cirrus. Deep convection is developing at this time over the SMO (Fig. 4), so that longwave cooling offsets shortwave heating in that region. At 1800 LT, net radiative heating reverts to a cooling throughout most of the lower troposphere, but there is still heating at the cirrus level over the GoC. By midnight, cooling returns throughout the entire column.

Inferences can also be made regarding the influence of radiative heating/cooling profiles on convection itself. Over the GoC, the maximum precipitation occurs during the early-morning hours (Fig. 6), coinciding well with the end of the period of maximum net upper-level cooling (Fig. 8), that is, when the time-integrated effects of this cooling would be strongest. The layer of maximum net cooling near 500 hPa resides atop a midlevel moist layer (Fig. 9). Similarly, the afternoon precipitation maximum over land (~1800 LT, Fig. 6) tends to coincide with the maximum in integrated shortwave heating at lower levels, lagging the peak by about 4 h (Fig. 8).

b. *Cross-gulf transects of convective heating and moistening rates*

The diurnal cycle of $Q_1 - Q_R$ for the 40-day NAME period is shown in Fig. 10. From (1), this quantity is principally a measure of the excess of condensation over evaporation since the divergence of eddy heat flux is typically small except in the upper troposphere (Houze 1982). Near sunrise (at 0600 LT), the results show weak net condensation in the upper troposphere, which may reflect the presence on some days of remnant anvil clouds from the previous day's convection and/or disturbed weather associated with GoC surges and easterly waves (Adams and Comrie 1997; Fuller and Stensrud 2000). Lang et al. (2007) and Rowe et al. (2008) show using S-Pol radar data that although minimal, some precipitation occasionally occurs over the high terrain during early morning hours. The weak heating peak near 800 hPa over the GoC is consistent with the ceilometer observations of Zuidema et al. (2007) showing a

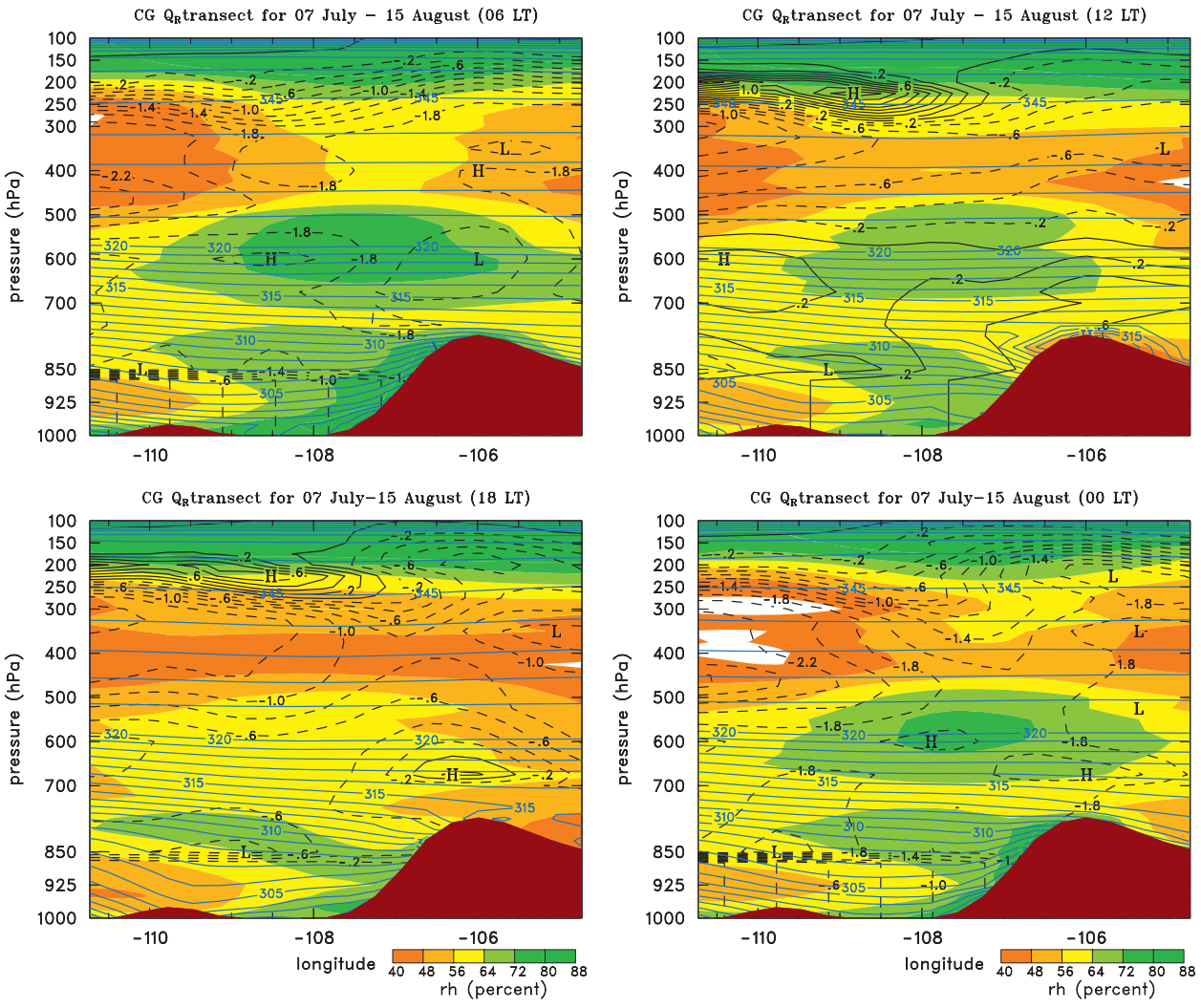

FIG. 9. Diurnal cycle of cross-gulf transect of net radiative heating rate (K day^{-1}, increment 0.2 K day^{-1}), relative humidity (scale at bottom), and isentropes (blue; 1-K increment below 320 K and 5 K above). Radiative heating rate is for 7 Jul–15 Aug 2004 for 10 yr (1998–2007) of TRMM. Other fields are for the 40-day NAME period.

cloudiness peak there in the early-morning hours. By noon, slightly stronger and more vertically aligned net condensation can be seen along the western slope of the SMO as convection develops at this time. By 1800 LT, strong net condensation ensues along the western slope peaking near 500 hPa, which is associated with intense precipitation (Fig. 4). Once again, the lack of deep moisture coincident with the column of deep heating is an artifact and reflects the absence of sounding data along the western slope. By midnight, there is a pattern of broad net condensational heating in the upper troposphere, peaking near 350 hPa, and net cooling in the lower troposphere. This change in the heating profile is consistent with a transition from deep convective heating to more stratiform precipitation, consistent with the findings of Nesbitt et al. (2008) and Rowe et al. (2008).

The diurnal cycle of Q_2 reflects a similar pattern of convective behavior (Fig. 11). Near sunrise (at 0600 LT), some moistening (negative Q_2) is evident in the lower troposphere over the SMO, indicating the presence of evaporation of light precipitation. This moistening reverts to a drying in the midtroposphere by noon, indicating the development of deep convection. The westward extension of drying over Baja is not viewed with confidence, although convection is known to break out over the Baja Peninsula mountain range during the daytime. At 1800 LT, strong drying is observed over the western slope of the SMO, consistent with intense precipitation at this time. Finally, by midnight, a pattern of drying aloft and moistening at low levels develops, reflecting the prevalence of stratiform precipitation.

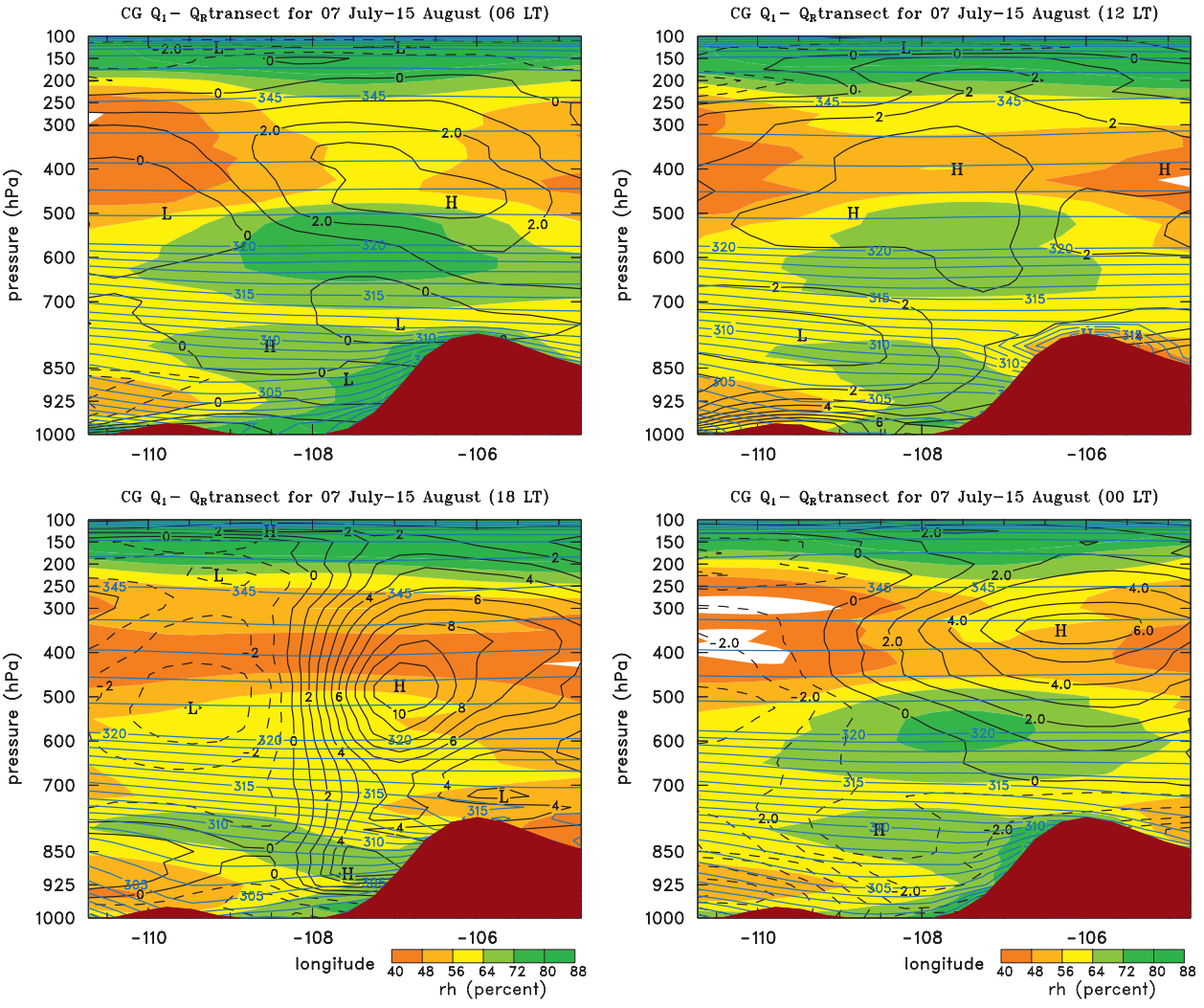

FIG. 10. Diurnal cycle of cross-gulf transect of $Q_1 - Q_R$ (K day^{-1}, increment 1 K day^{-1}), relative humidity (scale at bottom), and isentropes (blue; 1-K increment below 320 K and 5 K above). Radiative heating rate is for 7 Jul–15 Aug 2004 for 10 yr (1998–2007) of TRMM. Other fields are for the 40-day NAME period.

c. *Diurnal cycle of divergence, vertical motion, $Q_1 - Q_R$, and Q_2*

In Fig. 12, the diurnal cycle of divergence, vertical motion, $Q_1 - Q_R$, and Q_2 for 18 IOP days over the land portion of the EBA is shown. There is a trimodal structure to the divergence field, with a peak near 800 hPa (~2 km) during midmorning, another near 450 hPa (~6–7 km), and a third near 200 hPa (~12 km). Using S-Pol radar data, Rowe et al. (2008) found a trimodal distribution of echo-top heights, with peaks near 5, 9, and 12 km. The mid- and upper-tropospheric peaks in Fig. 12 could well correspond to the 5- and 12-km echo-top peaks found by Rowe et al. but there does not appear to be a separate peak near 9 km (300–350 hPa). However, the divergence aloft in Fig. 12 does extend over a deep layer, which could encompass the two echo-top maxima. The low-level peak in divergence near 800 hPa is presumably associated with shallow, nonprecipitating clouds, which would not be sampled by the S-Pol radar. This trimodal structure to the divergence, associated with inferred shallow, midlevel, and deep cloud populations, resembles cloud populations observed in the tropics (Johnson et al. 1999; Kikuchi and Takayabu 2004). The vertical motion, $Q_1 - Q_R$, and Q_2 diurnal cycles all show a similar pattern: deep convection developing in the afternoon, peaking near 1800 L, followed by stratiform-like profiles (e.g., heating aloft, cooling at low levels) just before and extending past midnight. The transition from deep convective to stratiform

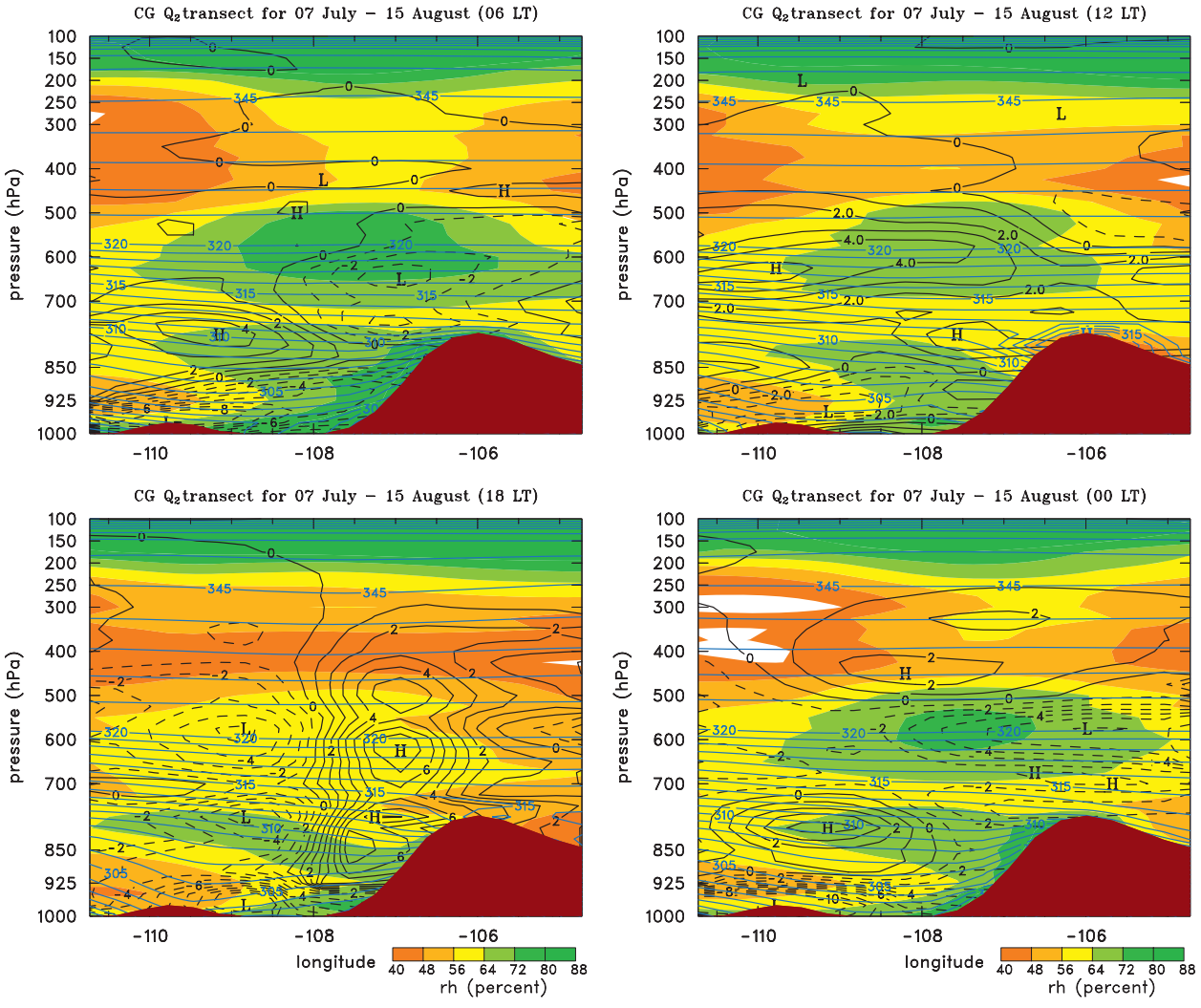

FIG. 11. Diurnal cycle of cross-gulf transect of Q_2 (K day^{-1}, increment 1 K day^{-1}), relative humidity (scale at bottom), and isentropes (blue; 1-K increment below 320 K and 5 K above). Radiative heating rate is for 7 Jul–15 Aug 2004 for 10 yr (1998–2007) of TRMM. Other fields are for the 40-day NAME period.

precipitation is accompanied by a shift from low-level convergence to midlevel convergence near the melting layer (550–600 hPa).

Results for the Gulf portion of the EBA, where there is minimal precipitation (Fig. 4), are shown in Fig. 13. During the daytime, the Gulf becomes a region of low-level divergence and subsidence as a result of diverging sea breeze flows toward the Baja peninsula and the SMO. Caution needs to be exercised in interpreting the profiles of $Q_1 - Q_R$ and Q_2 at the lowest levels where the vertical advection terms in (1) and (2) are small and the local change term dominates. Although the interior of the Gulf portion of the EBA resides over the water, the stations composing the array are over land (except for the R/V *Altair* at the mouth of the GoC) where there is a strong diurnal heating cycle. Therefore, the fields in the lowest kilometer or so are influenced by the boundary layer diurnal heating cycle. Above the boundary layer, the dominant feature in $Q_1 - Q_R$ is a heating maximum near 800 hPa just before midnight accompanied by a maximum in Q_2. This result indicates a maximum in precipitation near midnight, although the 4-h resolution of the soundings prevents a precise determination of the timing of this maximum. This finding is broadly consistent with the results in Fig. 6 and those of Zuidema et al. (2007), where the diurnal cycle of ceilometer-determined cloud-base heights at the R/V *Altair* located at the mouth of the GoC (Fig. 1) are presented. Their results show a maximum in the frequency of low-cloud bases

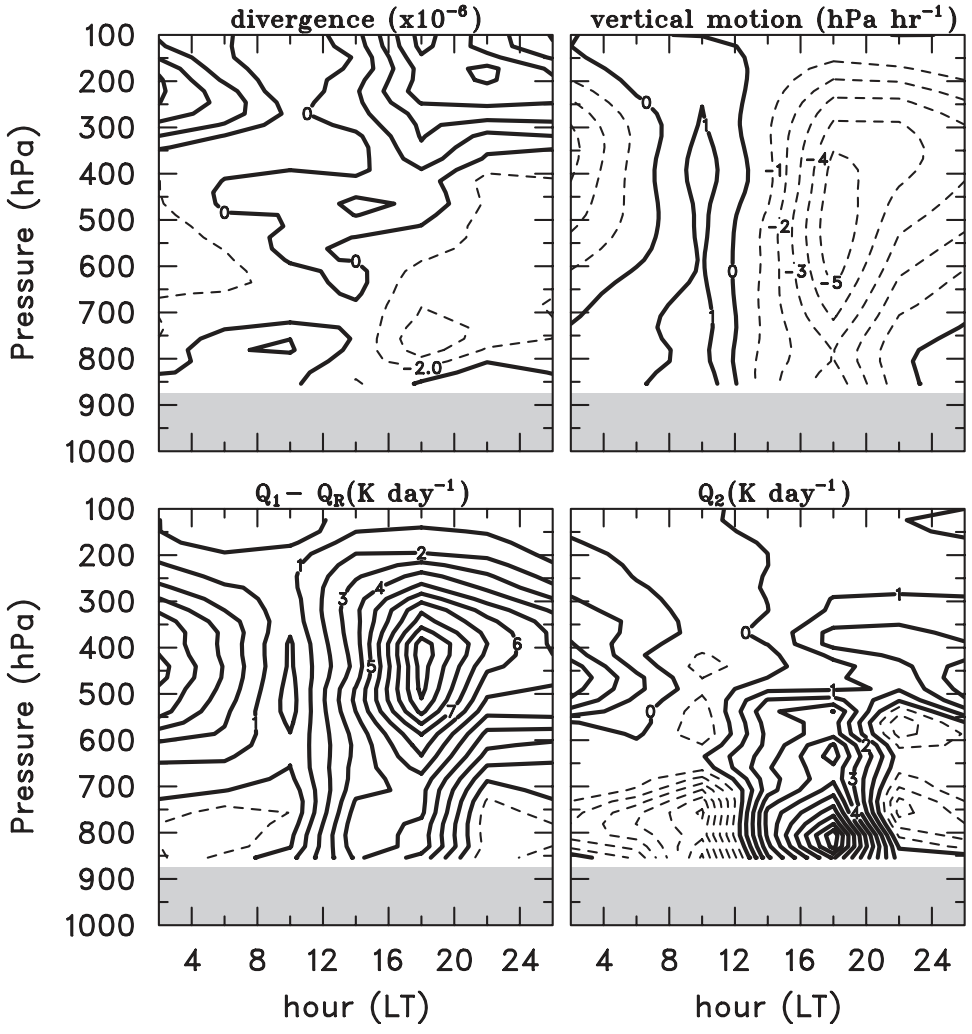

FIG. 12. Diurnal cycle of divergence (10^{-6} s^{-1}), vertical p velocity (hPa h^{-1}), and $Q_1 - Q_R$ and Q_2 (K day^{-1}) over land portion of EBA for 18 IOP days. Shaded area at bottom depicts average height of terrain.

beginning around midnight and continuing into the early-morning hours.

7. Discussion

This study focused on the mean diurnal cycle of latent heating and moistening by deep convection over the core NAME region during the 2004 summer monsoon. Despite limitations of the sounding network in terms of its density (Fig. 1) and launch frequency (4 day^{-1} for 22 days and 6 day^{-1} for 18 IOP days), the general pattern of the diurnal cycle of precipitation over this region is consistent with that diagnosed from radar and satellite observations (Lang et al. 2007; Nesbitt et al. 2008; Rowe et al. 2008). Specifically, the tropospheric heating and moistening distributions over land show on average shallow convection by late morning transitioning to deep convection in the late afternoon/evening, followed by stratiform precipitation near midnight. However, because the sounding sites were limited to stations along the coast and to the east of the SMO crest (Fig. 1), variations in the heating profiles within the EBA could not be determined. For example, the studies of Gochis et al. (2007), Lang et al. (2007), Nesbitt et al. (2008), and Rowe et al. (2008) suggest that convection over the highest terrain of the SMO is less deep than convection over the foothills, presumably as a result of reduced moisture and buoyancy. Because there were no sounding sites near the crest of the SMO or along the western slope, this variability could not be detected by the sounding network. Moreover, detailed sampling of the different propagating regimes within the range of S-Pol

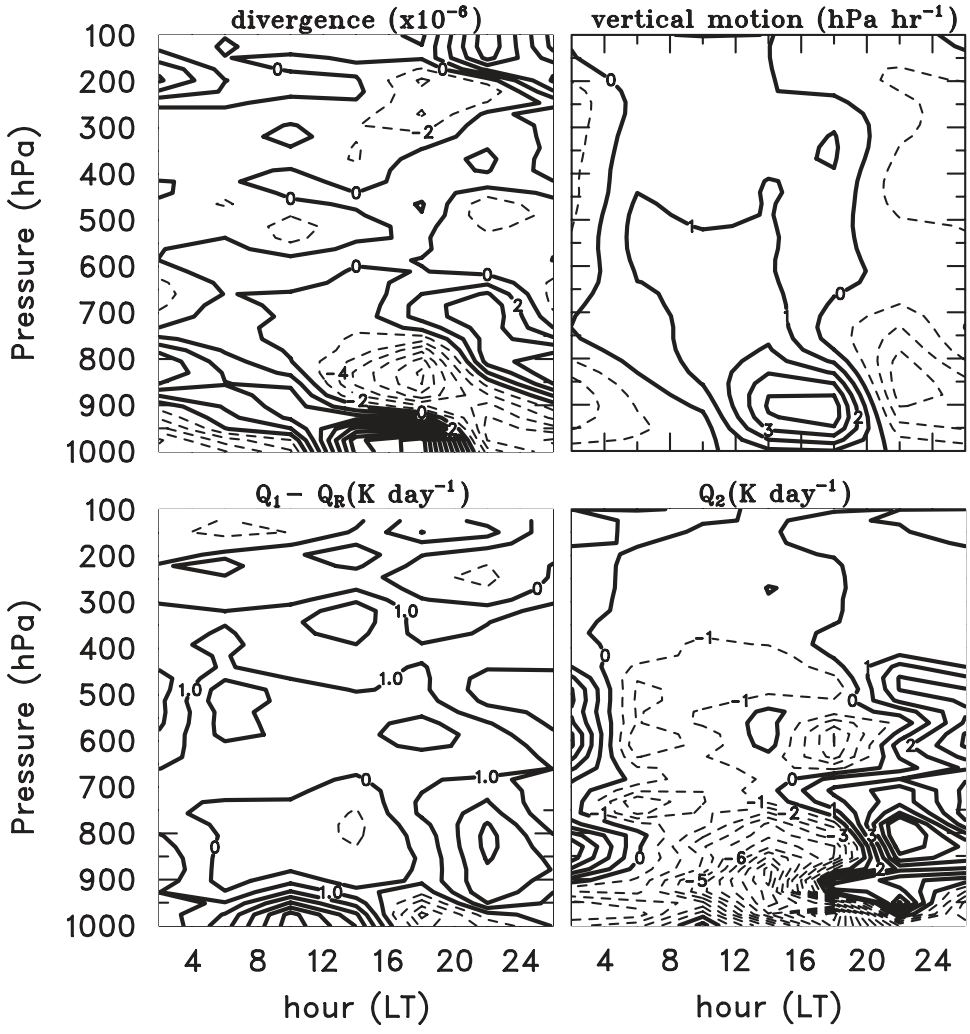

FIG. 13. Diurnal cycle of divergence (10^{-6} s^{-1}), vertical p velocity (hPa h^{-1}), and $Q_1 - Q_R$ and Q_2 (K day^{-1}) over GoC portion of EBA for 18 IOP days.

studied by Lang et al. (2007) could not be achieved with the sparse sounding network.

Nevertheless, a number of the aggregate features of convection over the SMO were sampled well by the gridded analysis. A summary of these findings is shown in Fig. 14, which presents the diurnal cycle of the amplitude of the maximum Q_1 in the column averaged over the land portion of the EBA (left panel) and the altitude of the highest Q_1 peak in the column (right panel). These figures combine results for both the 4 and 6 day^{-1} sounding cases. A prominent feature of both figures is the increasing convective activity from about noon into the evening hours. The average peak heating nearly triples over this time period and the heating peak rises from near 650 to 350 hPa. This behavior is consistent with the idea of shallow, weak convection around noon transitioning to intense, deep convection in the late afternoon and evening. Similar results can be interpreted from Fig. 12, but Fig. 14 also provides an indication of the statistical variability (standard deviation) of the characteristics of the heating at different times of day. Notably, the variability in the strength of the Q_1 peak is least during the midday hours, when presumably the development of convection is regularly controlled by a similar day-to-day pattern of insolation, whereas after convection develops, the local intensity is significantly modulated by subsequent outflow boundaries, cloud shading, mesoscale organization, and other factors, leading to greater variability at those times.

8. Summary and conclusions

This study has examined the diurnal heating and moistening cycles associated with deep convection in the

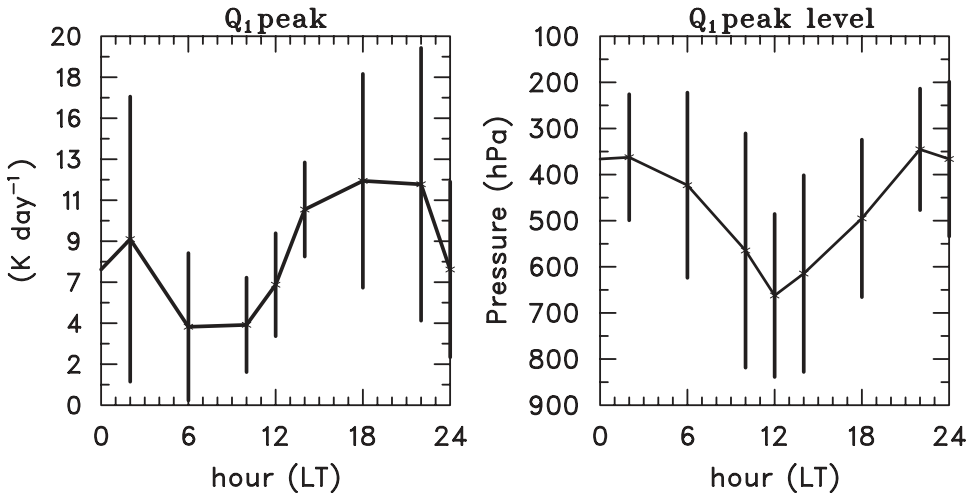

FIG. 14. (left) Diurnal cycle of maximum amplitude of Q_1 peak in column (K day^{-1}) over land portion of EBA. (right) Diurnal cycle of altitude of the highest Q_1 peak in the column. Data from four and six soundings per day have been combined. Vertical bars indicate standard deviations.

region of northwestern Mexico during the 2004 North American Monsoon Experiment. To better assess the latent heating effects in the apparent heat source Q_1, net radiative heating rate estimates were obtained for this region from the Hydrologic cycle and Earth's Radiation Budget (HERB) algorithm of L'Ecuyer and Stephens (2003, 2007). This approach has enabled estimates of $Q_1 - Q_R$ to be obtained, from which inferences of the net condensation rate can be made assuming the vertical divergence of the vertical eddy heat flux is small.

The principal results of this study are as follows:

- The incorporation of surface data, pibals, rawinsonde data, and wind profiler into a gridded sounding analysis over NAME Enhanced Budget Array (EBA) has resulted in a description of the diurnal cycle of the surface flow and tropospheric divergence, vertical motion, $Q_1 - Q_R$, and Q_2 determined with an accuracy heretofore not obtained in the North American monsoon region.
- There is an asymmetry in the development of daytime upslope flows across the Sierra Madre Occidental (SMO). By late morning, downslope surface flow still exists along the western slope of the SMO, while upslope flow has already begun on the eastern slope by this time. This asymmetry in the development of the upslope flows may be related to insolation asymmetry for the north–south SMO barrier and also to the presence of low-level clouds in the morning along the high western slopes, which may retard surface heating at that time (Ciesielski and Johnson 2008; Nesbitt et al. 2008).
- The vertical profiles of heating and moistening indicate, on average, shallow convection developing over the SMO around noon, transitioning to intense, deep convection in the late afternoon and evening. By midnight, the heating and moistening profiles are characteristic of stratiform precipitation (i.e., heating/drying in the upper troposphere and cooling/moistening in the lower troposphere).
- Results for the Gulf of California (GoC) portion of the EBA are strikingly different from those over land; namely, heating and moistening are confined principally to the lower troposphere below 700 hPa, peaking during the nighttime hours.
- The diurnal cycle of the net radiative heating rate is characterized by a net cooling during most of the daytime except for net heating in the lower and upper troposphere at midday. Net heating in the upper troposphere is seen over both land and ocean, but is more intense and at a lower level over the water. This difference can be explained by the fact that there is longwave cooling atop deep convection offsetting shortwave absorption over land, while over the ocean there is only thin cirrus aloft advected westward from deep convection over the SMO, yielding a net heating. There is also evidence that the time-integrated effects of mid- to upper-level net radiative cooling at night over the GoC contributes to the observed early-morning maximum in precipitation there. Moreover, the afternoon precipitation maximum over land (~1800 LT) tends to coincide with the maximum in integrated shortwave heating at lower levels, lagging the peak by about 4 h.
- As convection develops during the daytime, the amplitude of the average peak heating over the land portion of the EBA triples from noon to 1800 LT and the level of peak heating rises from 650 to 350 hPa,

reflecting both the intensification of convection and later the transition to stratiform precipitation.

The diurnal cycle of convection over the SMO is remarkably persistent from day to day, although its amplitude and degree of organization is modulated significantly by disturbances such as easterly waves, upper-level inverted troughs, and Gulf surges (Johnson et al. 2007; Lang et al. 2007). This study has not explored possible differences in heating and moistening profiles between undisturbed and disturbed days, but has examined the mean diurnal cycle during the summer monsoon season. Further stratification of the results is left for future study.

Acknowledgments. This research has been supported by the National Science Foundation, Mesoscale Dynamic Meteorology Program, under Grant. ATM-0639461 and the National Oceanic and Atmospheric Administration, Office of Global Programs, under Grant NA07OAR4310263. Michael Douglas is acknowledged for establishing the PACS-SONET pibal network and providing the pibal data for this study. We appreciate the assistance of Brian McNoldy with preparation of figures. The constructive comments of two anonymous reviewers are appreciated.

REFERENCES

Ackerman, T. P., K. Liou, F. P. J. Valero, and L. Pfister, 1988: Heating rates in tropical anvils. *J. Atmos. Sci.,* **45,** 1606–1623.

Adams, D. K., and A. C. Comrie, 1997: The North American monsoon. *Bull. Amer. Meteor. Soc.,* **78,** 2197–2213.

Aves, S. L., and R. H. Johnson, 2008: The diurnal cycle of convection over the northern South China Sea during the South China Sea Monsoon Experiment. *J. Meteor. Soc. Japan,* **86,** 919–934.

Barlow, M., S. Nigam, and E. H. Berbery, 1998: Evolution of the North American Monsoon System. *J. Climate,* **11,** 2238–2257.

Bechtold, P., J. P. Chaboureau, A. Beljaars, A. K. Betts, and M. Kohler, 2004: The simulation of the diurnal cycle of convective precipitation over land in a global model. *Quart. J. Roy. Meteor. Soc.,* **130,** 3119–3137.

Betts, A. K., and C. Jakob, 2002: Evaluation of the diurnal cycle of precipitation, surface thermodynamics, and surface fluxes in the ECMWF model using LBA data. *J. Geophys. Res.,* **107,** 8045, doi:10.1029/2001JD000427.

Carbone, R. E., J. D. Tuttle, D. A. Ahijevych, and S. B. Trier, 2002: Inferences of predictability associated with warm-season precipitation episodes. *J. Atmos. Sci.,* **59,** 2033–2056.

Chen, S. S., and R. A. Houze Jr., 1997: Diurnal variation and lifecycle of deep convective systems over the tropical Pacific warm pool. *Quart. J. Roy. Meteor. Soc.,* **123,** 357–388.

Ciesielski, P. E., and R. H. Johnson, 2006: Contrasting characteristics of convection over the northern and southern South China Sea during SCSMEX. *Mon. Wea. Rev.,* **134,** 1041–1062.

——, and ——, 2008: Diurnal cycle of surface flows during 2004 NAME and comparison to model reanalysis. *J. Climate,* **21,** 3890–3913.

——, ——, P. T. Haertel, and J. Wang, 2003: Corrected TOGA COARE sounding humidity data: Impact on diagnosed properties of convection and climate over the warm pool. *J. Climate,* **16,** 2370–2384.

——, ——, and J. Wang, 2009: Correction of humidity biases in Vaisala RS80-H sondes during NAME. *J. Atmos. Oceanic Technol.,* **26,** 1763–1780.

Dai, A. G., F. Giorgi, and K. E. Trenberth, 1999: Observed and model-simulated diurnal cycles of precipitation over the contiguous United States. *J. Geophys. Res.,* **104** (D6), 6377–6402.

Douglas, M. W., and J. Murillo, 2008: The Pan-American Climate Studies Sounding Network. *Bull. Amer. Meteor. Soc.,* **89,** 1709–1725.

——, R. A. Maddox, K. Howard, and S. Reyes, 1993: The Mexican monsoon. *J. Climate,* **6,** 1665–1677.

Fuller, R. D., and D. J. Stensrud, 2000: The relationship between tropical easterly waves and surges over the Gulf of California during the North American monsoon. *Mon. Wea. Rev.,* **128,** 2983–2989.

Gochis, D. J., J. C. Leal, C. J. Watts, W. J. Shuttleworth, and J. Garatuza-Payan, 2003: Preliminary diagnostics from a new event-based monitoring system network in support of the North American monsoon experiment (NAME). *J. Hydrometeor.,* **4,** 974–981.

——, C. J. Watts, J. Garatuza-Payan, and J. Cesar-Rodriguez, 2007: Spatial and temporal patterns of precipitation intensity as observed by the NAME event rain gauge network from 2002 to 2004. *J. Climate,* **20,** 1734–1750.

Gray, W. M., and R. W. Jacobson, 1977: Diurnal variation of deep cumulus convection. *Mon. Wea. Rev.,* **105,** 104–188.

Gutzler, D. S., and Coauthors, 2005: The North American Monsoon Model Assessment Project: Integrating numerical modeling into a field-based process study. *Bull. Amer. Meteor. Soc.,* **86,** 1423–1429.

Higgins, W., and Coauthors, 2006: The NAME 2004 field campaign and modeling strategy. *Bull. Amer. Meteor. Soc.,* **87,** 79–94.

Houze, R. A., Jr., 1982: Cloud clusters and large-scale vertical motions in the Tropics. *J. Meteor. Soc. Japan,* **60,** 396–410.

Huffman, G. J., and Coauthors, 2007: The TRMM Multisatellite Precipitation Analysis (TMPA): Quasi-global, multiyear, combined-sensor precipitation estimates at fine scales. *J. Hydrometeor.,* **8,** 38–55.

Janowiak, J. E., V. Kousky, and R. Joyce, 2005: Diurnal cycle of precipitation determined from the CMORPH high spatial and temporal resolution global precipitation analyses. *J. Geophys. Res.,* **110,** D23105, doi:10.1029/2005JD006156.

Johnson, R. H., 2006: Mesoscale processes. *The Asian Monsoon,* B. Wang, Ed., Praxis-Publishing Ltd., 331–356.

——, and P. E. Ciesielski, 2000: Rainfall and radiative heating rate estimates from TOGA-COARE atmospheric budgets. *J. Atmos. Sci.,* **57,** 1497–1514.

——, T. M. Rickenbach, S. A. Rutledge, P. E. Ciesielski, and W. H. Schubert, 1999: Trimodal characteristics of tropical convection. *J. Climate,* **12,** 2397–2433.

——, P. E. Ciesielski, B. D. McNoldy, P. J. Rogers, and R. K. Taft, 2007: Multiscale variability of the flow during the North American Monsoon Experiment. *J. Climate,* **20,** 1628–1648.

Khairoutdinov, M., and D. A. Randall, 2006: High-resolution simulations of shallow-to-deep convection transition over land. *J. Atmos. Sci.,* **63,** 3421–3436.

Kikuchi, K., and Y. N. Takayabu, 2004: The development of organized convection associated with the MJO during TOGA COARE IOP: Trimodal characteristics. *Geophys. Res. Lett.,* **31,** L10101, doi:10.1029/2004GL019601.

Kiladis, G. N., M. C. Wheeler, P. T. Haertel, K. H. Straub, and P. E. Roundy, 2009: Convectively coupled equatorial waves. *Rev. Geophys.,* **47,** RG2003, doi:10.1029/2008RG000266.

Kraus, E. B., 1963: The diurnal precipitation change over the sea. *J. Atmos. Sci.,* **20,** 551–556.

Krishnamurti, T. N., 1971: Tropical east–west circulations during the northern monsoon. *J. Atmos. Sci.,* **28,** 1342–1347.

——, and C. M. Kishtawal, 2000: A pronounced continental-scale diurnal mode of the Asian summer monsoon. *Mon. Wea. Rev.,* **128,** 462–473.

Lang, T. J., A. Ahijevych, S. W. Nesbitt, R. E. Carbone, S. A. Rutledge, and R. Cifelli, 2007: Radar-observed characteristics of precipitating systems during NAME 2004. *J. Climate,* **20,** 1713–1733.

L'Ecuyer, T. S., and G. L. Stephens, 2003: The tropical atmospheric energy budget from the TRMM perspective. Part I: Algorithm and uncertainties. *J. Climate,* **16,** 1967–1985.

——, and ——, 2007: The tropical atmospheric energy budget from the TRMM perspective. Part II: Evaluating GCM representations of the sensitivity of regional energy and water cycles to the 1998–99 ENSO cycle. *J. Climate,* **20,** 4548–4571.

——, and G. McGarragh, 2010: A 10-year climatology of tropical radiative heating and its vertical structure from TRMM observations. *J. Climate,* **23,** 519–541.

Liu, W. T., 2002: Progress in scatterometer application. *J. Oceanogr.,* **58,** 121–136.

Luo, H., and M. Yanai, 1984: The large-scale circulation and heat sources over the Tibetan Plateau and surrounding areas during the early summer of 1979. Part II: Heat and moisture budgets. *Mon. Wea. Rev.,* **112,** 966–989.

Madden, R. A., and P. R. Julian, 1971: Detection of a 40–50 oscillation in the zonal wind in the tropical Pacific. *J. Atmos. Sci.,* **28,** 702–708.

Mapes, B. E., T. T. Warner, and M. Xu, 2003: Diurnal patterns of rainfall in northwestern South America. Part III: Diurnal gravity waves and nocturnal offshore convection. *Mon. Wea. Rev.,* **131,** 830–844.

Mo, K. C., E. Rogers, W. Ebisuzaki, R. W. Higgins, J. Woollen, and M. L. Carrera, 2007: Influence of the North American Monsoon Experiment (NAME) 2004 enhanced soundings on NCEP operational analyses. *J. Climate,* **20,** 1821–1842.

Neale, R., and J. Slingo, 2003: The Maritime Continent and its role in the global climate: A GCM study. *J. Climate,* **16,** 834–848.

Negri, A. J., R. F. Adler, R. A. Maddox, K. W. Howard, and P. R. Keehn, 1993: A regional rainfall climatology over Mexico and the Southwest United States derived from passive microwave and geosynchronous infrared data. *J. Climate,* **6,** 2144–2161.

Nesbitt, S. W., D. J. Gochis, and T. J. Lang, 2008: The diurnal cycle of clouds and precipitation along the Sierra Madre Occidental during the North American Monsoon Experiment: Implications for precipitation estimation in complex terrain. *J. Hydrometeor.,* **9,** 728–743.

Nitta, T., 1983: Observational study of heat sources over the eastern Tibetan Plateau during the summer monsoon. *J. Meteor. Soc. Japan,* **61,** 590–605.

Nuss, W. A., and D. W. Titley, 1994: Use of multiquadric interpolation for meteorological objective analysis. *Mon. Wea. Rev.,* **122,** 1611–1631.

O'Brien, J. J., 1970: Alternative solutions to the classical vertical velocity problem. *J. Appl. Meteor.,* **9,** 197–203.

Randall, D. A., Harshvardhan, and D. A. Dazlich, 1991: Diurnal variability of the hydrological cycle in a general circulation model. *J. Atmos. Sci.,* **48,** 40–62.

Rowe, A. K., S. A. Rutledge, T. J. Lang, P. E. Ciesielski, and S. M. Saleeby, 2008: Elevation-dependent trends in precipitation observed during NAME. *Mon. Wea. Rev.,* **136,** 4962–4979.

Slingo, J., P. Inness, R. Neale, S. Woolnough, and G.-Y. Yang, 2003: Scale interactions on diurnal to seasonal timescales and their relevance to model systematic errors. *Ann. Geophys.,* **46,** 139–155.

Sperber, K. R., and T. Yasunari, 2006: Workshop on monsoon climate systems: Toward better prediction of the monsoon. *Bull. Amer. Meteor. Soc.,* **87,** 1399–1403.

Stensrud, D. J., R. L. Gall, S. L. Mullen, and K. W. Howard, 1995: Model climatology of the Mexican monsoon. *J. Climate,* **8,** 1775–1793.

Tang, M., and E. R. Reiter, 1984: Plateau monsoons of the Northern Hemisphere: A comparison between North America and Tibet. *Mon. Wea. Rev.,* **112,** 617–637.

Tucker, D. F., 1999: The summer plateau low pressure system of Mexico. *J. Climate,* **12,** 1002–1015.

Wallace, J., 1975: Diurnal variations in precipitation and thunderstorm frequency over the conterminous United States. *Mon. Wea. Rev.,* **103,** 406–419.

Webster, P. J., and G. L. Stephens, 1980: Tropical upper-tropospheric extended clouds: Inferences from winter MONEX. *J. Atmos. Sci.,* **37,** 1521–1541.

——, and Coauthors, 2002: The JASMINE pilot study. *Bull. Amer. Meteor. Soc.,* **83,** 1603–1630.

Yanai, M., S. Esbensen, and J. H. Chu, 1973: Determination of bulk properties of tropical cloud clusters from large-scale heat and moisture budgets. *J. Atmos. Sci.,* **30,** 611–627.

Yang, G. Y., and J. Slingo, 2001: The diurnal cycle in the tropics. *Mon. Wea. Rev.,* **129,** 784–801.

Zuidema, P., C. Fairall, L. Hartten, J. Hare, and D. Wolfe, 2007: On air–sea interaction at the mouth of the Gulf of California. *J. Climate,* **20,** 1649–1661.